ELSEVIER

Optics and Lasers in Engineering 40 (2003) 81–90

OPTICS and LASERS in ENGINEERING

Study of a vibrating plate: comparison between experimental (ESPI) and analytical results

G. Romero[a,*], L. Alvarez[b,c], E. Alanís[b], L. Nallim[a,d], R. Grossi[a]

[a] *Facultad Ingeniería, Universidad Nacional de Salta, Buenos Aires 177, 4400 Salta, Argentina*
[b] *Facultad Cs. Exactas, Universidad Nacional de Salta, Buenos Aires 177, 4400 Salta, Argentina*
[c] *Becaria CIUNSa, Universidad Nacional de Salta, Buenos Aires 177, 4400 Salta, Argentina*
[d] *Becaria CONICET, Universidad Nacional de Salta, Buenos Aires 177, 4400 Salta, Argentina*

Abstract

Real-time electronic speckle pattern interferometry (ESPI) was used for tuning and visualization of natural frequencies of a trapezoidal plate. The plate was excited to resonant vibration by a sinusoidal acoustical source, which provided a continuous range of audio frequencies. Fringe patterns produced during the time-average recording of the vibrating plate—corresponding to several resonant frequencies—were registered. From these interferograms, calculations of vibrational amplitudes by means of zero-order Bessel functions were performed in some particular cases. The system was also studied analytically. The analytical approach developed is based on the Rayleigh–Ritz method and on the use of non-orthogonal right triangular co-ordinates. The deflection of the plate is approximated by a set of beam characteristic orthogonal polynomials generated by using the Gram–Schmidt procedure. A high degree of correlation between computational analysis and experimental results was observed.

Keywords: Speckle interferometry; ESPI; Vibration; Computational analysis

1. Introduction

Electronic speckle pattern interferometry (ESPI) is a useful tool to carry out non-destructive tests in a variety of fields such as optical metrology [1–4], industrial process control, visual inspection line, etc. The technique is well suited to measure deformations in mechanical systems subjected to stress under several boundary conditions [5]. Particularly, the visualization and measurement of the mechanical

*Corresponding author.
E-mail address: marigra@unsa.edu.ar (G. Romero).

0143-8166/03/$ - see front matter
PII: S0143-8166(02)00058-1

vibration of elastic objects is one of the most useful applications. Vibration problems have been extensively studied by means of computational methods, which provide approximate solutions. The Rayleigh–Ritz method is a powerful computational technique applicable to a variety of engineering problems [6,7].

In many cases, experimental and computational methods can be combined so that the data obtained by one method can be used by the other one to verify the results [8]. In this paper we are interested in comparing the results obtained by means of a computational method with those obtained experimentally using time-average speckle interferometry. As a test object we used a trapezoidal plate, mounted in cantilever, subjected to a periodic load and excited to different resonant vibrations by a sinusoidal acoustic source. Real-time displays of interference fringe patterns allow high precision tuning of normal modes of vibration, so that measurement of the corresponding resonant frequencies can be done. Once the resonant mode is attained, images of the fringe pattern are recorded and stored for later analysis and comparison with the predicted computational solutions.

2. Experimental set-up

The experimental set-up for time-average recording of ESPI is depicted in Fig. 1. One beam of a split He–Ne laser light is expanded and collimated by lens L_1 and

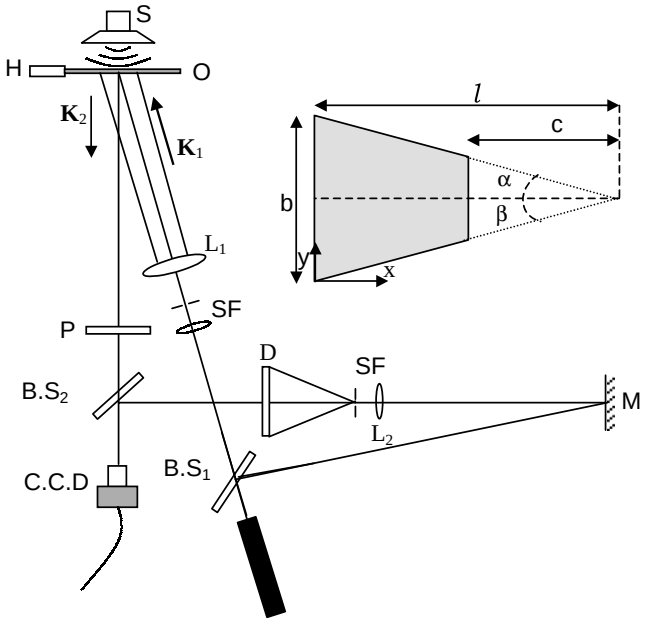

Fig. 1. Experimental set-up: O, object; S, speaker; H, holder; P polarizer; BS_1, BS_2, beam splitter; D, diffuser; SF, spatial filter; M, mirror; L_1, collimating lens; CCD, digital camera. The inset shows the plate and its dimensions.

illuminates the object surface. In the figure, vectors $\boldsymbol{K}_1$ and $\boldsymbol{K}_2$ define the illumination and observation directions, respectively. The other beam is expanded and passes through a diffuser D, which results in the speckled reference beam. The light dispersed by the object and the reference beam are brought together by the beamsplitter BS_2 and directed to the CCD camera. To improve the contrast, a polarizer P is put on the object beam path behind the beamsplitter BS_2. The object is a trapezoidal plate of constant thickness, with geometrical parameters indicated in the inset. The plate is clamped on the left edge and acoustically stressed by the speaker S, driven by a variable frequency sine wave function generator.

3. Measurement of resonant frequencies

At the beginning of one experiment, when the object is stationary in equilibrium, irradiances $I_0(x, y)$, produced by interference of the object and reference field, are recorded by the CCD camera and stored in the frame grabber memory. This irradiance equals

$$I_0(x,y) = I_{ob}(x,y) + I_{re}(x,y) + 2[I_{ob}(x,y)I_{re}(x,y)]^{1/2}\cos[\varphi(x,y)], \tag{1}$$

where $I_{ob}(x, y)$ and $I_{re}(x, y)$ are the intensities at the co-ordinate (x, y) of the object and reference beam, respectively and $\varphi(x, y)$ is the phase difference between the two interfering beams, which is assumed to be randomly distributed.

When the object is vibrating sinusoidally in one of its resonant modes, at a single frequency f, the phase change of the object beam is given by

$$\theta(x,y,t) = k(x,y)\sin 2\pi ft \quad \text{where } k(x,y) = 4\pi a(x,y)/\lambda \tag{2}$$

(if $\boldsymbol{K}_1 = -\boldsymbol{K}_2$, i.e. with normal illumination and viewing directions) in which $a(x, y)$ is the vibration amplitude at the object point (x, y) and λ is the laser light wavelength. Irradiances $I(x, y, t)$ result from the interference of the time varying object field and the reference field. If the TV frame integration time is much longer than the vibration period, as is the case in these experiments, the irradiances will be time averaged during the exposure time and can be written as

$$I_{av}(x,y) = I_{ob}(x,y) + I_{re}(x,y) + 2(I_{ob}(x,y)I_{re}(x,y))^{1/2}\cos\varphi(x,y)J_0[k(x,y)], \tag{3}$$

in which J_0 is a zero-order Bessel function of the first kind. This frame is recorded and subtracted from the stored reference frame, $I_0(x, y)$, and displayed in real time on the TV monitor. This procedure provides time-averaged information about the vibration amplitude resulting in a fringe pattern in the form of a Bessel function, as it will be derived in Section 5.

Fringes of constant speckle contrast represent regions of constant amplitude vibration on the object surface. A resonant condition of the object is easily achieved by looking at the fringes displayed on the monitor while tuning the audio generator

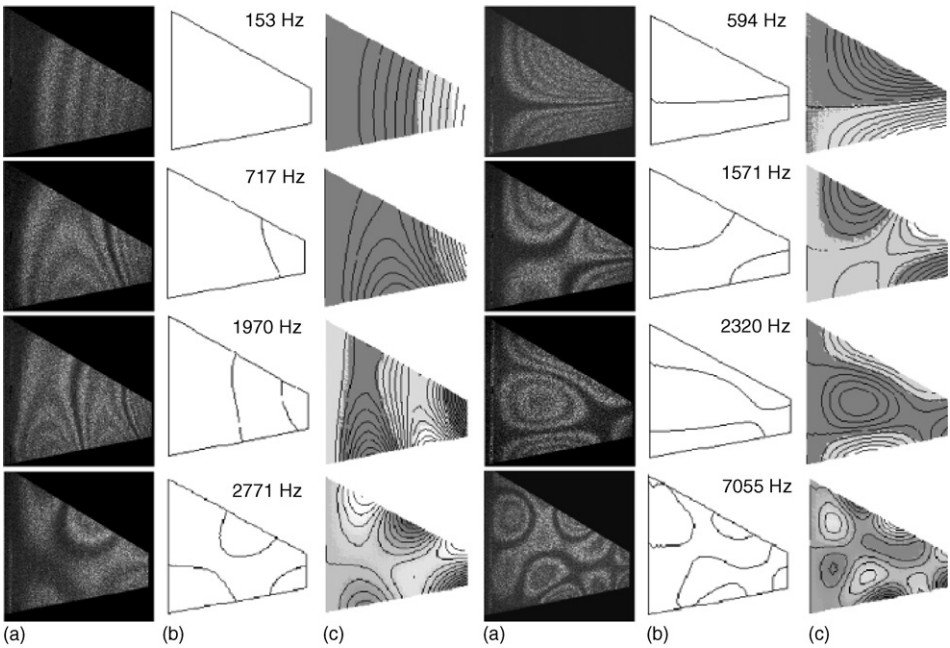

Fig. 2. From left to right: (a) interferograms; (b) calculated nodal patterns; and (c) calculated modal shapes. The corresponding resonant frequencies are indicated on each diagram.

until a stationary fringe pattern is observed. Once this condition is attained, the resonant frequency is measured from the signal generator, previously calibrated by means of an oscilloscope.

In Fig. 2, several interferograms corresponding to different resonant frequencies are shown. Several fringes of different speckle contrast can be seen, each one representing regions of constant vibration amplitudes. Dark fringes represent nodal regions. In the figure, it is also possible to observe, on the right of each interferogram, the nodal patterns obtained by means of the Ritz method, in conjunction with a set of beam characteristic orthogonal polynomials as approximating functions, representing the modal shapes of the plate. It can be seen a remarkable agreement between the calculated modal shapes and the corresponding fringe pattern. Resonant frequencies are indicated in each diagram.

4. Resonant frequencies calculation

The analytical method distinguishes each resonant mode by means of a dimensionless frequency parameter Ω, which takes into account the geometrical shape and boundary condition of the modelled object. The assumed shape functions

for using the Rayleigh–Ritz procedure are give by

$$W(x,y) = \sum_i \sum_j c_{ij} p_i(x) q_j(y), \tag{4}$$

where $p_i(x)$ and $q_j(y)$ are the orthogonal polynomials, and c_{ij} are the arbitrary coefficients which are to be determined. Bhat [9,10] has developed the procedure for the construction of the orthogonal polynomials. The maximum kinetic energy of the freely vibrating plate with amplitude $W(x,y)$ and radian frequency ω is given by

$$T_{\max} = \frac{h\rho\omega^2}{2} \int \int_R W^2(x,y)\, \mathrm{d}x\, \mathrm{d}y, \tag{5}$$

where ρ is the mass density of the plate material, h is the plate thickness and the integration is carried out over the entire plate domain R. The maximum strain energy of the plate is given by

$$U_{\max} = \frac{1}{2} \int \int_R D \left\{ \left(\frac{\partial^2 W}{\partial x^2} + \frac{\partial^2 W}{\partial y^2} \right)^2 - 2(1-\mu) \left[\frac{\partial^2 W}{\partial x^2} \frac{\partial^2 W}{\partial y^2} - \left(\frac{\partial^2 W}{\partial x \partial y} \right)^2 \right] \right\} \mathrm{d}x\, \mathrm{d}y, \tag{6}$$

where D is the flexural rigidity and is given by

$$D = \frac{Eh^3}{12(1-\mu^2)}, \tag{7}$$

where E is the Young's modulo and μ is the Poisson's ratio.

The natural frequencies are obtained from the Rayleigh quotient [11] as

$$\omega^2 = \frac{U_{\max}}{T_{\max}}. \tag{8}$$

Minimization of the Rayleigh quotient with respect to each parameter c_{ij}, leads to the necessary conditions

$$\frac{\partial \omega^2}{\partial c_{ij}} = 0. \tag{9}$$

Substituting the approximating function, Eq. (4), into Eq. (9) leads to the governing eigenvalue equation

$$\sum_i \sum_j (K_{ijkh} - \Omega^2 M_{ijkh}) c_{ij} = 0, \tag{10}$$

where Ω is the dimensionless frequency parameter, K_{ijkh} involves integrals of products of the shape functions and their derivatives and M_{ijkh} involves integrals of products of the shape functions and values deriving from the kinetic energy contribution of any point mass. Back substitution yields the coefficient vectors and, finally, substitution of these coefficient vectors into Eq. (4) gives the mode shapes of the plates.

Table 1
Geometrical and mechanical parameters of the test object

$h = 0.98 \times 10^{-3}$	m
$\mu = 0.35$	
$E = 6.82 \times 10^{10}$	N/m^2
$D = 6.1$	N m
$l = 0.116$	m
$\rho = 2.86 \times 10^{3}$	kg/m^3

Table 1
Geometrical and mechanical parameters of the test object

The resonant frequencies of the real object are related to the parameter Ω by means of the expression

$$\Omega = \sqrt{\frac{\rho h}{D}}\,\omega l^2,$$

therefore,

$$f = \Omega\left(\frac{1}{2\pi l^2}\sqrt{\frac{D}{\rho h}}\right), \tag{11}$$

where f is the frequency in Hz and l is a characteristic objet length (see Fig. 1). The values of the geometrical and mechanical properties of the test object used in this work are given in Table 1.

Values of the frequencies measured experimentally in the preceding section and the corresponding values calculated by the analytical method and Eq. (11), are compared in Fig. 3. A linear relation between calculated and measured frequencies with a high degree of correlation ($r^2 = 0.9998$) can be seen. The main errors of the measured frequencies arise from the appreciation on the signal generator scale. These are estimated to be 1% approximately. From the observed linear relation a bound of errors of the same type can be assigned to the dimensionless frequency parameter determined analytically. Nevertheless, the slope of the regression line is 0.975, differing from the ideal unit slope by 2.5%. This difference is attributed to the measured parameters involved in the constant factor of Eq. (11), which are estimated to be 2% approximately.

5. Amplitude measurement

As indicated in Section 3, the interferograms represent the difference between $I_0(x, y)$ and $I_{av}(x, y)$, given by Eqs. (1) and (3), respectively. Omitting the (x, y) coordinates the result can be written as

$$|I_{av} - I_0| = |2(I_{ob}I_{re})^{1/2}[1 - J_0(k)]\cos\varphi|, \tag{12}$$

that is, the speckled background is modulated by the factor $[1 - J_0(k)]$. The centres of bright and dark fringes correspond to the maxima and minima of this factor, respectively. Note that this factor is similar to the characteristic function that

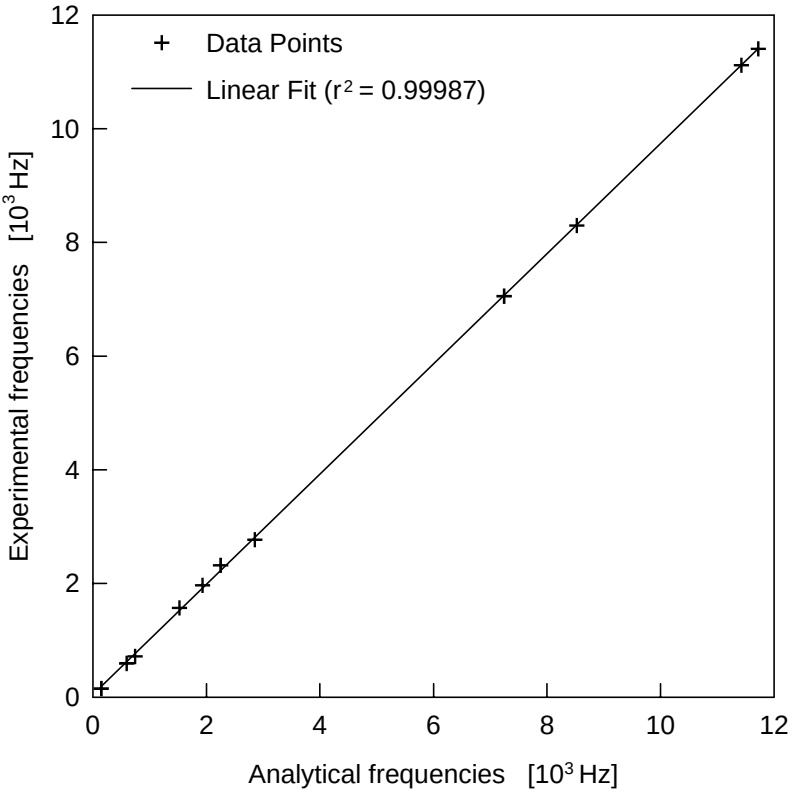

Fig. 3. Correlation between measured and calculated frequencies for 11 resonant modes.

describes real-time, time-average holographic interferometry [2]. From Eq. (2) the vibration amplitude can be calculated as

$$a(x,y) = k(x,y)\lambda/4\pi, \tag{13}$$

in which $k(x,y)$ are the values of the argument of the Bessel function corresponding to its extrema. Zero-order dark fringes appear when the intensity value, given by Eq. (12), is zero. This condition corresponds to $k = 0$ ($[1 - J_0(k)] = 0$) and, from Eq. (13), the vibration amplitude is also zero, representing nodal regions. The fringes contrast decrease quickly starting from the zeroth order on.

Comparisons between measured and calculated deformation of the plate were carried out. As the experiment was not designed to obtain the full field vibration amplitude—in which case a phase step method, among others, should be more appropriate [12]—only a few particular directions along the object were chosen to perform vibration amplitude measurements. Let us take as an example the interferogram corresponding to a resonant frequency of 2320 Hz, as shown in Fig. 2. The image was processed in the Fourier domain to filter out high frequencies

due to speckle noise. To minimize the errors introduced due to the sharp edges of the plate, a technique to extrapolate the fringes beyond the boundary of the object was employed. The resulting image is shown in Fig. 4(a), where a particular direction is indicated. Along this direction the corresponding fringes profile, shown in Fig. 4(b), was analysed in order to localize the co-ordinates of the centre of bright and dark fringes. By applying Eq. (13), the corresponding amplitude of vibration was calculated. The results are shown in Fig. 4(c), together with the curve calculated by means of the analytical method, using Eq. (4). Note that the analytically derived shape of the plate can be used to remove the sign ambiguity in fringe order numbers.

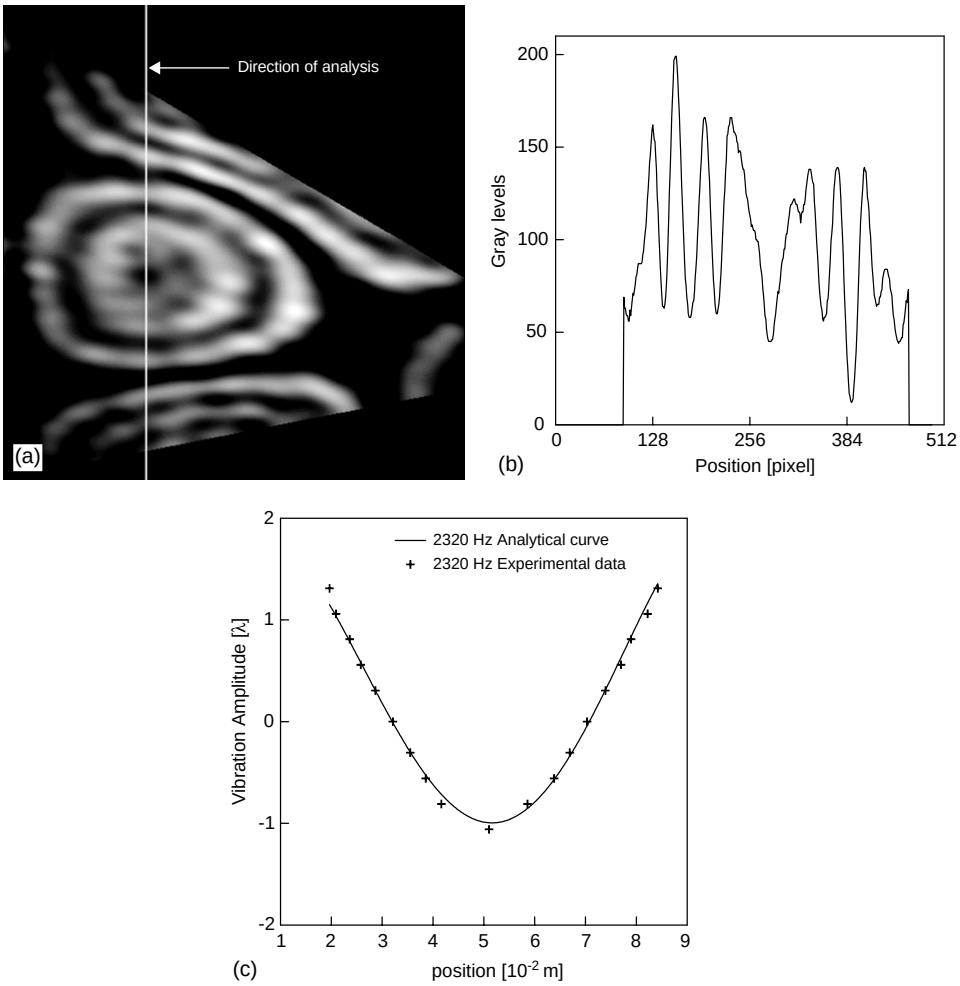

Fig. 4. (a) Filtered interferogram corresponding to a resonant frequency of 2320 Hz; (b) fringe profile along the direction indicated in (a); and (c) comparison between amplitudes calculated by analytical and experimental methods.

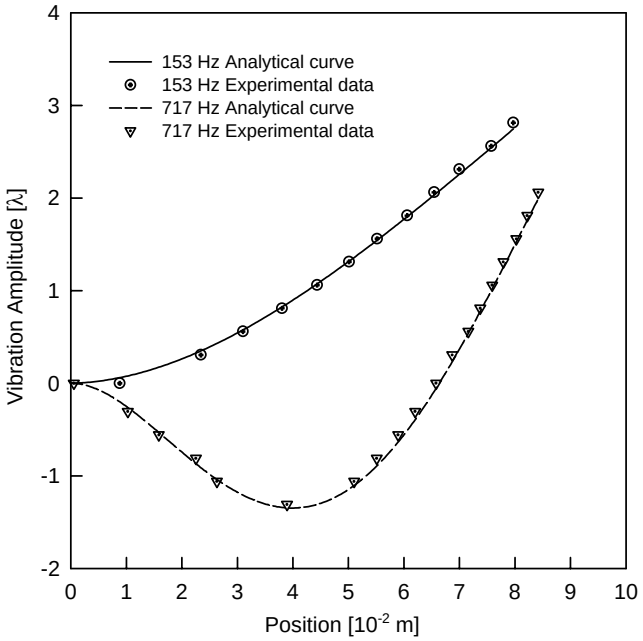

Fig. 5. Comparison between amplitudes calculated by analytical and experimental methods, respectively, for the resonant frequencies 153 and 717 Hz.

As the energy of excitation is unknown, the analytical curve has been multiplied by a constant for comparison purposes. This constant was determined by means of an iteration process to minimize the mean deviation between the two sets of data. A mean deviation of 0.06λ was found representing approximately 2% of the full deflection of the plate. The localization of the nodal points, given by the analytical and experimental method, differs by 1.5% considering the distance between them.

Similar calculations were performed for the resonant frequencies 153 and 717 Hz, respectively. In Fig. 5, measured and calculated amplitudes for these cases are compared.

6. Conclusions

We have presented a study of a vibrating plate, in which analytical solution and experimental measurements are compared. Several modes of vibration have been visualized by means of a standard ESPI technique. The experimental set-up is very simple to implement and shows great sensitivity for tuning the resonant frequencies. Values of the resonant frequencies, obtained by both analytical and experimental methods are closely correlated taking into account the estimated errors in the measurements of the involved parameters. Qualitatively, the visualized mode shapes

as well as the nodal patterns match remarkably with the predictions of the computational method. As noted in Section 5, the contrast of the fringes decreases quickly from the zero order on; thus, limiting the number of fringes of useful visibility. However, amplitude measurements have also been carried out experimentally for a few particular cases, and they showed a reasonable agreement with the analytical results.

Acknowledgements

This work was supported by "Consejo de Investigación" (Project No. 832), "Facultad de Ciencias Exactas" and "Facultad de Ingeniería" of UNSa.

References

[1] Ennos E. Speckle interferometry. In: Dainty JC, editor. Laser speckle and related phenomena, vol. 9. Berlin: Springer, 1984. p. 203–53.
[2] Vest CM. Measurement of mechanical vibrations. In: Ballard SS, editor. Holographic interferometry. New York: Wiley, 1979 [Chapter 4].
[3] Torroba R, Joenathan C. Real time refractive index measurements by ESPI. Lamp Series Report, Miramare Trieste, 1991.
[4] Pomarico J, Torroba R. Focal lengths measurements using digital speckle interferometry. Opt Commun. 1997;141:1–4.
[5] Jüptner W. Principles of direct holography for interferometry. In: Jüptner W, Osten W, editors. Proceedings of the Second International Workshop on Automatic Processing of Fringe Patterns—Fringe'93. Berlin: Akademie Verlag, 1993. p. 115–20.
[6] Grossi R, Bhat R. Natural frequencies of edge restrained trapezoidal rectangular plates. J Sound Vib 1995;185(2;):335–43.
[7] Liew KM, Lam KY. A Rayleigh–Ritz approach to transverse vibration of isotropic and anisotropic trapezoidal plates using orthogonal plate functions. Int. J. Solids Struct 1991;27(2):189–203.
[8] Pryputniewicz R. Experiment and FEM modeling. In: Jüptner W, Osten W, editors. Proceedings of the Second International Workshop on Automatic Processing of Fringe Patterns—Fringe'93. Berlin: Akademie Verlag, 1993. p. 275–9.
[9] Bhat RB. Natural frequencies of rectangular plates using characteristic orthogonal polynomials in Rayleigh–Ritz method. J Sound Vib 1985;102:493–9.
[10] Bhat RB. Plate deflection using orthogonal polynomials. J Eng Mech 1985;101:1301–9.
[11] Grossi RO. On the use of the Rayleigh–Schmidt approach. J Ind Math Soc 1990;40(2):115–22.
[12] Wang LS, Krishnaswamy S. Aditive-substractive speckle interferometry: extraction of phase data in noisy environments. Opt Eng 1996;35(3):794–801.